

Polarisation, Born Effective Charges, and Topological Invariants via a Berry-Phase Approach

Christian Carbogno^{*1,2}, Nikita Rybin^{1,3}, Sara Panahian Jand¹, Alaa Akkoush^{1,4}, Carlos Mera Acosta^{1,5,6}, Zhenkun Yuan¹, and Mariana Rossi⁴

¹The NOMAD Laboratory at the Fritz-Haber-Institut der Max-Planck-Gesellschaft Faradayweg 4-6, 14195, Berlin, Germany

²Current address: Theory Department, Fritz Haber Institute of the Max Planck Society, Faradayweg 4-6, 14195 Berlin, Germany

³Current address: Skolkovo Institute of Science and Technology, Bolshoi bulvar 30, build.1, 121205, Moscow, Russia

⁴Max Planck Institute for the Structure and Dynamics of Matter, 22761 Hamburg, Germany

⁵Center for Natural and Human Sciences, Federal University of ABC, Santo André, SP, Brazil

⁶Current address: Faculty of Engineering, University of La Sabana, Chía 250001, Colombia

Summary

The Berry connection $\mathbf{A}_{mn}(\mathbf{k})$, the Berry curvature $\nabla \times \mathbf{A}_{mn}(\mathbf{k})$, and the Berry phase $\varphi = \oint \mathbf{A}_{mn}(\mathbf{k}) \cdot d\mathbf{k}$ are key properties describing the reciprocal-space topology, here the connection between two electronic states labeled m and n . They provide a profound link between the phase of a quantum wave function and macroscopic observables as well as material properties. Most prominently, these quantities are central to our understanding of topological materials and provide a route to classify phases in terms of topology [1]. For instance, all the aforementioned quantities enter the definition of the topological-invariant \mathbb{Z}_2 as given by Fu and Kane [2]:

$$\mathbb{Z}_2 = \frac{1}{2\pi} \sum_n^{\text{occ}} \left\{ \oint_{\partial B} \mathbf{A}_{nn}(\mathbf{k}) \cdot d\mathbf{k} - \int_B [\nabla \times \mathbf{A}_{nn}(\mathbf{k})] d^2\mathbf{k} \right\} \text{ mod } 2 \quad (1)$$

Here, B is half the Brillouin zone (BZ) and ∂B its boundary, the sum runs over all occupied states, and the gauge of $\mathbf{A}_{nm}(\mathbf{k})$ is constrained to respect time-reversal symmetry.

Furthermore, these quantities play a fundamental role for computing the polarization in periodic systems [3, 4], or, more precisely, for calculating the polarization density \mathbf{P} and its derivatives, the Born effective charges Z_I^* , via

$$\mathbf{P} = \frac{1}{V} \left[\sum_I Z_I \mathbf{R}_I - \frac{eV}{(2\pi)^3} \sum_n^{\text{occ}} \int_{\text{BZ}} \mathbf{A}_{nn}(\mathbf{k}) d^3\mathbf{k} \right] \text{ mod } \mathbf{P}_0 \quad \text{and} \quad Z_{\alpha,I\beta}^* = \frac{V}{e} \frac{\partial P_\alpha}{\partial R_{I\beta}}. \quad (2)$$

Here, V denotes the volume of the unit cell, $\mathbf{P}_0 = \frac{e}{V}(|\mathbf{a}_1|, |\mathbf{a}_2|, |\mathbf{a}_3|)$ the polarization quanta along the lattice vectors \mathbf{a}_α , Z_I the nuclear charge, \mathbf{R}_I the nuclear positions, and e the elementary charge. The first term describes the trivial contribution of the bare nuclei, whereas the second term covers the

*carbogno@fhi-berlin.mpg.de

contributions stemming from the electronic states $\Psi_n(\mathbf{k})$. Besides providing the theoretical foundation for understanding the quantization of adiabatic charge transport [5], the polarization is a key property for describing the electrodynamics in solids, e.g., for modeling light-matter interactions and for studying ferroelectric and piezoelectric effects.

In addition, these quantities play a central role in the assessment of currents, fluxes, magnetization, and, last but not least, in the transformation of delocalized electronic wave functions into a localized Wannier basis [6, 7, 8]. We refer the interested reader to Ref. [9] for a more throughout discussion of all these effects.

Current Status of the Implementation

To compute all the aforementioned material properties, the fundamental quantity that needs to be calculated in a first-principles code is the Berry connection [6]:

$$A_{mn}(\mathbf{k}) = i \langle u_m(\mathbf{k}) | \partial u_n(\mathbf{k}) / \partial \mathbf{k} \rangle . \quad (3)$$

Here, $u_l(\mathbf{k}) = \exp(-i\mathbf{k}\mathbf{r})\Psi_l(\mathbf{k}, \mathbf{r})$ is the lattice-periodic part of the electronic wave function $\Psi_l(\mathbf{k}, \mathbf{r})$ for state l with wave vector \mathbf{k} and $\langle \cdot | \cdot \rangle$ denotes the scalar product in Hilbert space. Before evaluating this definition, let us remind that FHI-aims uses a Bloch-like representation of the wave functions

$$\Psi_n(\mathbf{k}, \mathbf{r}) = \sum_{\mu} C_{\mu}(n, \mathbf{k}) \chi_{\mu}(\mathbf{k}, \mathbf{r}) \quad \text{with} \quad \chi_{\mu}(\mathbf{k}, \mathbf{r}) = \sum_N \exp(i\mathbf{k}\mathbf{L}_N) \phi_{\mu,N}(\mathbf{r} - \mathbf{R}_{\mu} - \mathbf{L}_N) , \quad (4)$$

as detailed in Contrib. 1.1. Here, $C_{\mu}(n, \mathbf{k})$ are the Kohn-Sham expansion coefficients and $\phi_{\mu,N}(\mathbf{r} - \mathbf{R}_{\mu} - \mathbf{L}_N)$ are the numeric atomic orbitals (NAOs) associated to the basis function with index μ for the periodic image in the cell \mathbf{L}_N of the atom located at \mathbf{R}_{μ} . With that, the Berry connection can be expressed as

$$A_{mn}(\mathbf{k}) = \underbrace{i \sum_{\nu} \sum_{\mu} C_{\nu,n}^*(\mathbf{k}) \frac{\partial C_{\mu,n}(\mathbf{k})}{\partial \mathbf{k}} S_{\mu\nu}(\mathbf{k})}_{A_{mn}^{(1)}(\mathbf{k})} - \underbrace{\sum_{\nu} \sum_{\mu} C_{\nu,n}^*(\mathbf{k}) C_{\mu,n}(\mathbf{k}) [D_{\mu,\nu}(\mathbf{k}) - \mathbf{R}_{\mu} S_{\mu\nu}(\mathbf{k})]}_{A_{mn}^{(2)}(\mathbf{k})} . \quad (5)$$

The first term in Eq. (5), i.e., $\mathbf{A}_{mn}^{(1)}(\mathbf{k})$, denotes the gauge-dependent Berry-connection term, which here includes the overlap matrix $S_{\mu\nu}(\mathbf{k}) = \sum_N e^{i\mathbf{k}\mathbf{L}_N} \langle \phi_{\nu,0} | \phi_{\mu,N} \rangle$ due to the non-orthogonality of the employed NAO basis set. For evaluating the associated contribution to the Berry phase, i.e., the closed-path integrals required for Eq. (1) and Eq. (2), the reciprocal-space path is discretized on K points $(\mathbf{k}_1, \mathbf{k}_2, \dots, \mathbf{k}_K)$, whereby the initial and final point are equivalent with respect to the BZ's periodicity $\mathbf{k}_1 = \mathbf{k}_K \bmod \frac{2\pi}{V}$. By expressing the \mathbf{k} -derivatives as two-point finite-differences, one obtains [7]

$$\sum_n^{\text{occ}} \oint_{\text{BZ}} \mathbf{A}_{nn}^{(1)}(\mathbf{k}) \cdot d\mathbf{k} = -\text{Im} \ln \left[\det (\underline{\mathbf{M}}_{0,1} \cdot \underline{\mathbf{M}}_{1,2} \cdots \underline{\mathbf{M}}_{K-2,K-1} \cdot \underline{\mathbf{M}}_{K-1,0}) \right] . \quad (6)$$

Note that the Kohn-Sham coefficients $\underline{\mathbf{C}}^{\text{occ}}(\mathbf{k})$ used for computing the matrices

$$\underline{\mathbf{M}}_{a,b} = \underline{\mathbf{C}}^{\text{occ}\dagger}(\mathbf{k}_a) \underline{\mathbf{S}}(\mathbf{k}_a) \underline{\mathbf{C}}^{\text{occ}}(\mathbf{k}_b)$$

entering the above expression only cover the subspace of occupied states.

The second term entering Eq. (5), i.e., $\mathbf{A}_{mn}^{(2)}(\mathbf{k})$, is gauge-invariant and features the matrix

$$D_{\mu\nu}(\mathbf{k}) = - \sum_N e^{i\mathbf{k}\mathbf{L}_N} \langle \phi_{\nu,0} | [\mathbf{r} - \mathbf{R}_\mu - \mathbf{L}_N] | \phi_{\mu,N} \rangle, \quad (7)$$

which captures the contributions of the NAO basis functions. Since this form exhibits the exact same periodicity as the overlap matrix $\underline{\mathbf{S}}(\mathbf{k})$, it can be integrated up using the real-space routines already present in FHI-aims [10, 11]. Similarly, the associated contribution to the Berry-phase required for Eq. (1) and Eq. (2) can be computed straightforwardly by performing the trace over occupied states and by numerically integrating $A_{mn}^{(2)}(\mathbf{k})$ along the exact same path used in Eq. (6).

In the current implementation, the polarization is calculated in the basis of the reciprocal-lattice vectors. To perform the \mathbf{k} -derivative along the reciprocal-lattice vector of interest, the closed-loop path is chosen parallel to it. The remaining integrations $\int d^2\mathbf{k}$ perpendicular to this path are performed by splining the Berry phases. As an example for such a calculation, Fig. 1 shows the polarization of PbTiO_3 , here for smoothly interpolated geometries and lattices between the tetragonal, symmetry-degenerate $P4mm$ equilibrium structures and the cubic, centrosymmetric $Pm\bar{3}m$ structure. While the latter structure must have a vanishing polarization due to symmetry, the tetragonal configurations do not. This highlights that the absolute values of the polarization are meaningless, only relative differences of the polarization matter. To evaluate such differences, “branch-matching” [12], i.e., ensuring that the actual polarization values lay on the branch associated to the same multiples of \mathbf{P}_0 value, is crucial¹.

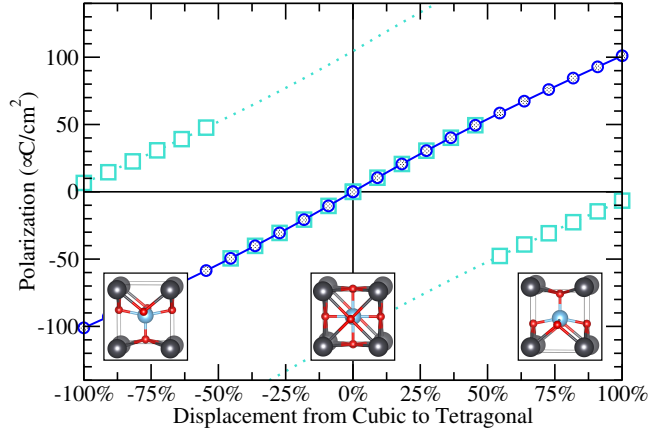


Figure 1: Polarisation ($24 \times 8 \times 8$ \mathbf{k} -points for the Berry-phase) of PbTiO_3 (HSE06, 8^3 \mathbf{k} -points) along the minimum-energy path connecting the tetragonal, symmetry-degenerate $P4mm$ and the cubic, centrosymmetric $Pm\bar{3}m$ structure. Cyan squares denote the bare output, blue circles the “branch-matched” polarization, for which the discontinuities associated to the mod \mathbf{P}_0 -operation are resolved.

For the evaluation of the \mathbb{Z}_2 invariant, the current implementation follows the formalism proposed in Refs. [16, 17], which is equivalent to the definition given in Eq. (1), but does not require gauge-fixing. In practice, it requires to track the evolution of the individual Wannier centers

$$\mathbf{X}_n(\mathbf{k}_2) = \oint_{-\pi}^{\pi} A_{nn}(\mathbf{k}_1) \cdot d\mathbf{k}_1 \quad \text{mod } 2\pi \quad (8)$$

across a path in the BZ described by \mathbf{k}_2 . In practice, one evaluates the line-path integral in Eq. (8) for varying values of \mathbf{k}_2 . Each of these integrals is solved for all occupied states as discussed above, i.e., by using $A_{mn}^{(1)}(\mathbf{k})$ as given by Eq. (6) and $A_{mn}^{(2)}(\mathbf{k})$ along a discretized path $\mathbf{k}_1 \perp \mathbf{k}_2$. The determinant viz. trace is, however, not evaluated. Rather, the obtained matrix is diagonalized and the complex phase of the resulting eigenvalues is then tracked, as the example in Fig. 2 shows. If an arbitrary continuous line across the whole \mathbf{k}_2 -axis crosses the evolution of the Wannier centers an even number of times \mathbb{Z}_2 is 0 and otherwise 1. Similarly, this can be judged by tracking the largest gap between the individual

¹Note that an internal branch matching in FHI-aims is already performed for splining and integrating over the perpendicular \mathbf{k} -directions.

Wannier centers [16].

Usability and Tutorials

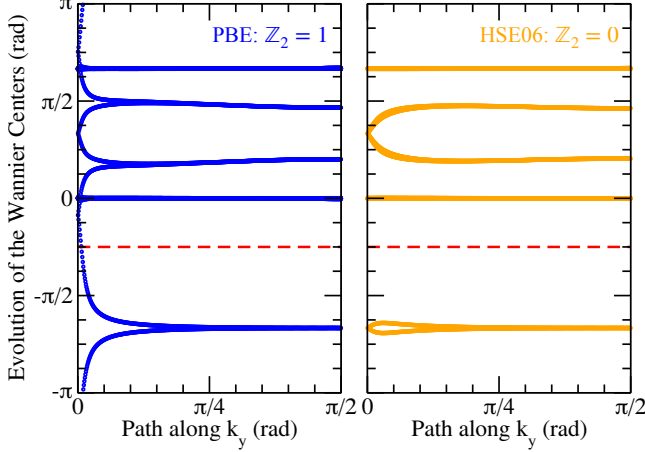


Figure 2: Evolution of the Wannier Centers of Charge for the functionalized 2D-honeycomb structure of GeF_2 , as computed with PBE (left) and HSE06 (right) along $\mathbf{k}_2 = k_y$. Both calculations use spin-orbit coupling [13]. As indicated by the red, dashed line, a continuous path along k_y must cross the Wannier Centers an odd (PBE) viz. even (HSE06) number of times, resulting in $\mathbb{Z}_2 = 1$ and $\mathbb{Z}_2 = 0$, respectively. This showcases the influence of the exchange-correlation functional on topological invariants [14, 15].

ferences. Although these functionalities are rather self-explanatory, a tutorial is provided at <https://fhi-aims-club.gitlab.io/tutorials/phonons-with-fhi-vibes/>, which also showcases how the computed Born effective charges can be used to account for long-range dipole interactions in the calculations of phonon spectra in polar crystals, see [18] and references therein.

Similarly, the evaluation of \mathbb{Z}_2 viz. of the evolution of the Wannier centers of charge only requires to add one keyword to the `control.in` file:

```
output Z2_invariant  $\gamma$   $n_{\parallel}$   $n_{\perp}$ 
```

Here, γ is an index that encodes which Cartesian planes shall actually be targeted, e.g. $\gamma = 1$ implies that Eq. (8) is evaluated along the first reciprocal-lattice vector using a \mathbf{k} -discretization of n_{\parallel} points and that this procedure is repeated for n_{\perp} closed-paths that have equidistant $k_2 \in [0, \pi]$ and $k_3 = 0$. The latter scan over k_2 can, for instance, be used to discern strong from weak topological insulators [19].

Eventually, let us note that the implementation supports all exchange-correlation functionals, i.e., all semi-local and hybrid functionals, as well as spin-orbit coupling as described in Ref. [13]. Also, given that this functionality targets unit cells and requires rather dense \mathbf{k} -grids the parallelization occurs over \mathbf{k} -points using LAPACK for the compute-intense linear-algebra operations.

For the evaluation of the polarization, it is sufficient to add one keyword to the `control.in` file:

```
output polarization  $\alpha$   $n_1$   $n_2$   $n_3$ 
```

For instance, the line `output polarization 2 5 10 5` will compute the polarization along the reciprocal-lattice vector number 2 using a grid of $5 \times 10 \times 5$ \mathbf{k} -points in the BZ. As the example highlights, the discretization used along the reciprocal-lattice vector of interest, i.e., the one along which the closed-path integral in Eq. (6) is performed, usually requires denser grids. For convenience, multiple output polarization statements can be combined and, if all three directions are requested, the code will also report the polarization in Cartesian coordinates. For the evaluation of Born effective charges \underline{Z}_I , a Python script `BEC.py` is provided in the utilities folder of the FHI-aims distribution to perform the required derivatives, cf. (2) via finite dif-

Future Plans and Challenges

So far, the existing implementation has proven useful, accurate, and performant for targeting relatively simple materials with few (< 100) atoms in the unit cell. However, there is increased scientific and technological interest in targeting materials with structural or compositional disorder, e.g., for alloyed topological insulators featuring thousands of atoms in the unit cell [20]. For such kind of systems, the current k -point-based parallelization strategy is not efficient. Rather, support for distributed linear algebra (ScaLAPACK) is needed and is currently being pursued.

Furthermore, the described Berry-phase approach does not only give access to polarization, Born effective charges, and topological invariants, but to a multitude of other material properties, as described in the introduction. In this context, a systematic interface between the methodologies described in this contribution and the density-functional perturbation theory implementation described in Contrib. 5.1 is desirable for the accelerated assessment of response properties, e.g., piezoelectric tensors, but also Born effective charges, or other properties pivotal for electrodynamics viz. light-matter interactions. Another route that is being exploited is the machine-learning of the polarization for systems with a reduced number of atoms using a local representation. These simulations allow us to treat much larger unit cells. While learning the polarization requires care because of dealing with a topological quantity [21], our goal is to target models that can be used in the context of nuclear dynamics with light-matter coupling, as reported in Ref. [22]. Finally, let us emphasize that the implemented infrastructure also makes a transformation to Wannier functions straightforward. While this functionality would not be particularly useful with FHI-aims itself, given that the NAOs already provide a localized representation, it would be beneficial for interfacing to other community codes based on a Wannier representation. For instance, this would give access to all the functionality provided by, e.g., Wannier90 [23], EPW [24], and Perturbo [25], and, in turn, enable more systematic, community-wide benchmarks and collaborations across “code-boundaries”.

References

- [1] A. Bansil, H. Lin, and T. Das, *Rev. Mod. Phys.* **88**, 021004, (2016).
- [2] L. Fu and C. L. Kane, *Phys. Rev. B* **74**, 195312, (2006).
- [3] R. Resta, *Ferroelec.* **136**, 51 (1992).
- [4] R. D. King-Smith and D. Vanderbilt, *Phys. Rev. B* **47**, 1651 (1993).
- [5] D. J. Thouless, *Phys. Rev. B* **27**, 6083 (1983).
- [6] E. I. Blount, *Solid State Phys.* **13**, 305 (1962).
- [7] N. Marzari and D. Vanderbilt, *Phys. Rev. B* **56**, 12847 (1997).
- [8] N. Marzari, A. A. Mostofi, J. R. Yates, I. Souza, and D. Vanderbilt, *Rev. Mod. Phys.* **84**, 1419 (2012).
- [9] D. Vanderbilt, *Berry Phases in Electronic Structure Theory*, Cambridge University Press (2018).
- [10] V. Havu, V. Blum, P. Havu, and M. Scheffler, *J. Comp. Phys.* **228**, 8367 (2009).
- [11] F. Knuth, C. Carbogno, V. Atalla, V. Blum, and M. Scheffler, *Comput. Phys. Commun.* **190**, 33 (2015).
- [12] N. A. Spaldin, *J. Sol. Stat. Chem.* **195**, 2 (2012).
- [13] W. P. Huhn and V. Blum, *Phys. Rev. Mater.* **1**, 033803, 08 (2017).
- [14] C. Si, J. Liu, Y. Xu, J. Wu, B.-L. Gu, and W. Duan, *Phys. Rev. B* **89**, 115429, (2014).

- [15] L. Matthes, S. Kűfner, J. Furthműller, and F. Bechstedt, *Phys. Rev. B* **94**, 085410, 08 (2016).
- [16] A. A. Soluyanov and D. Vanderbilt, *Phys. Rev. B* **83**, 235401, 06 (2011).
- [17] R. Yu, X. L. Qi, A. Bernevig, Z. Fang, and X. Dai, *Phys. Rev. B* **84**, 075119, 08 (2011).
- [18] S. Baroni, S. de Gironcoli, and A. Dal Corso, *Rev. Mod. Phys.* **73**, 515 (2001).
- [19] L. Fu, C. L. Kane, and E. J. Mele, *Phys. Rev. Lett.* **98**, 106803, (2007).
- [20] G. Cao *et al.*, *Phys. Rev. Mater.* **4**, 034204, 03 (2020).
- [21] P. Xie, Y. Chen, W. E, and R. Car, *arXiv*, **2205.11839** (2022).
- [22] Y. Litman *et al.*, *J. Chem. Phys.* **161**, 062504, (2024).
- [23] G. Pizzi *et al.*, *J. Phys.: Cond. Matt.* **32**, 165902, (2020).
- [24] S. Ponce, E. R. Margine, C. Verdi, and F. Giustino, *Comput. Phys. Commun.* **209**, 116 (2016).
- [25] J.-J. Zhou, J. Park, I.-T. Lu, I. Maliyov, X. Tong, and M. Bernardi, *Comp. Phys. Comm.* **264**, 107970, (2021).